Received: 4 September 2023 | Revised: 5 June 2024 | Accepted: 9 June 2024

DOI: 10.1002/eqe.4183

RESEARCH ARTICLE

WILEY

Shake table tests of steel moment resisting frame with self-centering SMA-based isolators

Jiahao Huang[1] | **Songye Zhu**[1] | **Bin Wang**[2] | **Zhi-peng Chen**[1]

[1]Department of Civil and Environmental Engineering, The Hong Kong Polytechnic University, Hong Kong, China

[2]Key Laboratory of Deep Earth Science and Engineering, Sichuan University, Chengdu, China

Correspondence
Songye Zhu, Department of Civil and Environmental Engineering, The Hong Kong Polytechnic University, Hong Kong, China.
Email: ceszhu@polyu.edu.hk

Funding information
Hong Kong PhD Fellowship Scheme; Joint Research Centre for Marine Infrastructure, Grant/Award Number: 1-CEB0; Hong Kong Branch of National Rail Transit Electrification and Automation Engineering Technology Research Center, Grant/Award Number: K-BBY1; Research Grants Council, University Grants Committee, Grant/Award Number: 15231723

Abstract

This paper investigates a steel moment resisting frame (MRF) with a novel type of self-centering (SC) base isolators, wherein superelastic shape memory alloy (SMA) U-shaped dampers (SMAUDs) work as core components. A two-story steel MRF model equipped with two SMAUD-based isolators was designed and built in the laboratory, and a series of shake table tests were conducted to examine the dynamic behavior and seismic performance of the frame. Throughout all the tests, no interventions, such as repair or replacement of frame or isolator members, were done. Shake table test results demonstrated that the SMAUD-based isolators could withstand multiple strong earthquakes with stable SC behavior. The utilization of SMAUD-based isolators provided effective protection for the frame, enabling it to restore its original position with minimal structural damage. A numerical model of the tested steel MRF with SMAUD-based isolators was also built. The results obtained from the numerical analyses agreed with those of the shake table tests satisfactorily. A comparative study of the seismic performance between the MRF with SMAUD-based isolators and the MRF with traditional steel U-shaped damper-based isolators was also conducted in the shake table tests. The results showed that SMAUD-based isolators not only inherit the isolation function of conventional isolators to protect the frame but also possess an SC ability to eliminate residual isolator deformation effectively. Moreover, SMAUD-based isolators demonstrate remarkable resilience to withstand multiple strong seismic events without any need for repair or replacement.

KEYWORDS

moment resisting frame, numerical simulation, seismic base isolation, self-centering, shake table test, shape memory alloy

1 | INTRODUCTION

Catastrophic earthquakes have caused extensive damage to diverse urban and rural infrastructure globally. For example, the 1994 Northridge and 1995 Kobe earthquakes caused unexpectedly brittle fractures and residual deformations in steel moment resisting frames (MRFs), revealing vulnerabilities of these structures.[1,2] Such seismic devastation has galvanized worldwide efforts over recent decades to develop and implement advanced seismic hazard mitigation strategies for a full range of infrastructure types. Among these strategies, seismic base isolators have been regarded as a successful approach in protecting various buildings and structures against earthquakes.[3,4]

Seismic base isolators play a crucial role in reducing seismic forces transmitted to a superstructure by partially decoupling it from its foundation. The protection is achieved by elongating structural fundamental period and increasing structural damping. Conventional seismic base isolators, such as elastomeric and sliding bearings, are characterized by low lateral stiffness or friction, leading to the concentration of earthquake-induced displacements within the base isolators.[5] Some researchers incorporated metallic yield dampers into base isolators to enhance seismic energy dissipation. For example, Nippon Steel Co.[6] adopted steel U-shaped dampers (SUDs) in base isolators that exhibited stable hysteretic behavior. Ene et al.[7] investigated the behavior of base isolators with SUDs subjected to bidirectional loading. Typically, these base isolators undergo considerable displacements during earthquakes and experience substantial residual deformation after unloading. Notably, excessive residual deformation of base isolators can jeopardize the operational functions of buildings and the functionality of nonstructural components passing the isolation layer, such as misalignment of electrical and plumbing systems and damage to waterproofing layers.[8,9] Additionally, the effectiveness of base isolators could be compromised during immediate aftershocks and future earthquakes. In view that excessive residual deformation can result in severe economic losses and increased repair costs,[10] the self-centering (SC) concept that aims to minimize structural residual deformation has emerged. In conventional base isolators, the SC capability can be achieved in two ways: relying on elastic components (e.g., rubber)[11] or on the concave configuration of a sliding surface in a friction pendulum to provide restoring forces.[3,12] However, the SC performance of the conventional base isolators is likely diminished by the hysteretic behavior of energy dissipation parts, such as the inelastic deformation of the lead cores in lead rubber bearings. Existing studies have shown that the insufficient SC ability of conventional base isolation systems can result in excessive residual deformation under seismic motions, especially in the case of near-field seismic motions characterized by long periods and large velocity pulses.[13,14] Consequently, concern about the SC capability of traditional base isolation systems has been raised. To address these concerns, Constantinou et al.[15] proposed a base isolation system equipped with a fluid-restoring force device to eliminate the residual displacement. Lee et al.[16] developed a roller seismic isolator employing cylindrical rollers placed on V-shaped inclined planes, which could achieve SC capability after earthquakes.

Recently, damping devices incorporating shape memory alloy (SMA) elements have gained increasing popularity in the realm of earthquake engineering.[17–19] With superelasticity and energy dissipation ability, SMAs can recover their initial shapes with the removal of external loads and exhibit flag-shaped hysteresis behavior under cyclic loading. Consequently, SMA-based devices can provide dual functions, namely SC and moderate energy dissipation, which is appealing in seismic resilient designs to eliminate residual deformation of structures after earthquakes. Various kinds of SMA-based structural components have already been proposed and investigated in the past two decades, including SMA braces,[20–22] SC SMA connections,[23–25] and SMA dampers.[26,27] Additionally, as the prevailing SMA material employed, NiTi SMAs exhibit high resistance to corrosion and fatigue.[28] These favorable characteristics make SMAs appealing for use in seismic-resilient, lifecycle-sustainable infrastructure design.

In addition to the extensive research conducted on existing SMA-based structural components, some researchers investigated the integration of SMA elements into base isolation systems, capitalizing on the superelasticity of SMAs to enhance the SC capability of base isolators. In the early days, many proof-of-concept studies focused on isolators incorporating SMA wires. For example, Dolce et al.[29] developed isolation devices utilizing SMA wires, which exhibited excellent SC ability under cyclic loading. Choi et al.[30] introduced SMA wires into elastomeric bearings to form a novel type of isolation device. In addition to SMA wires, isolators with alternative types of SMA elements have been proposed. Casciati et al.[31] conducted shake table tests on a base isolator prototype equipped with SMA bars. Attanasi and Auricchio[32] introduced a flat sliding bearing installed with SMA helical springs as a SC lateral restraining system. Fang et al.[33] incorporated SMA ring springs into the bridge restrainers.

The existing research on SMA-based seismic protection devices primarily concentrates on the utilization of SMA wires[19,34,35] and bars,[23,24,36] employing their uniaxial tensile behavior. However, in the case of isolation devices incorporating SMA wires, satisfying the desired elongation for the design displacement requires lengthy SMA wires and careful

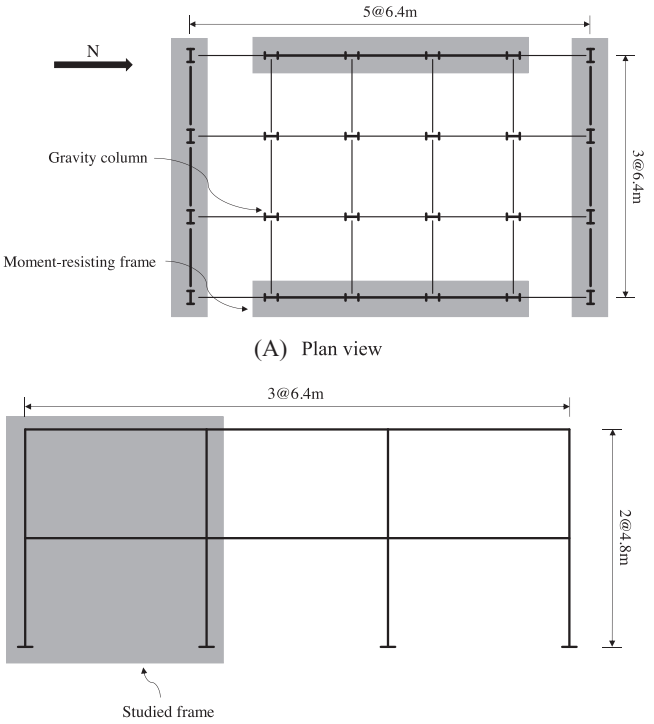

FIGURE 1 Prototype frame.

consideration of uniform deformation along the entire length. This requirement substantially increases the configuration complexity of the isolators. Despite the remarkable research on the adoption of the uniaxial behavior of SMAs, research regarding the application of other mechanical behaviors of SMAs in earthquake engineering remains notably limited.

Recently, Wang et al.[37] introduced a novel kind of SC base isolator equipped with SMA U-shaped dampers (SMAUDs). Unlike conventional seismic base isolators, this new isolator can provide unique SC capability and moderate energy dissipation by utilizing the flexural behavior of SMAUDs. Although the superior performance of SC isolators with SMAUDs has been illustrated through quasi-static isolator tests,[37] the seismic-resilient performance of multistory frame structures equipped with these SC SMAUD-based isolators subjected to earthquakes has not been experimentally validated prior to this paper. To bridge this research gap, this paper presents the shake table tests of a 1/4-scaled two-story, one-bay steel MRF equipped with novel SC base isolators utilizing SMAUDs as the key components. First, a scaled two-story, one-bay steel MRF equipped with SMAUD-based isolators was designed. Prior to installation in the tested MRF, the performance of the isolators was characterized through cyclic loading tests. Then, the dynamic responses of the MRF with SMAUD-based isolators subjected to two series of incremental ground motions were evaluated. Numerical simulations of the tested MRF were also conducted and compared with the results of the shake table tests, validating that the MRF equipped with SMAUD-based isolators could exhibit superior seismic performance under multiple seismic hazard levels. To provide a comparative study, the performance of the MRF with SMAUD-based isolators is presented together with that of the MRF equipped with SUD-based isolators.

2 | TESTED FRAME

2.1 | Prototype frame

To investigate the performance of a steel structure with base isolators, a prototype steel MRF was designed by following AISC 341-16 and ASCE 7–16.[38,39] Figure 1 shows the plan and elevation views of the prototype MRF, a two-story steel frame consisting of numerous bays in each direction. The story height and bay width of the prototype MRF are 4.8 and 6.4 m, respectively. In each direction, six MRF bays are specifically designed to resist seismic lateral loads, while other

TABLE 1 Seismic design parameters of the prototype frame.

Design parameters	Value
Mapped spectral acceleration of short-periods, S_S	2.0 g
Mapped spectral acceleration of 1-sec period, S_1	0.72 g
Site coefficients	$F_a = 1.0$, $F_v = 1.5$
Damping coefficients	$B_s = 1.0$, $B_1 = 1.0$
Seismic design category	D
Redundancy factor	1.3
Occupancy category	II
Importance factor	1
Damping ratio	5%
Response modification coefficient, R	8
Overstrength factor, Ω_0	3
Deflection amplification factor, C_d	5.5

TABLE 2 Scale ratios of similitude laws.

Parameters	Similitude relation	Scaling ratio
Length	S_L	1/4
Modulus of elasticity	S_E	1
Acceleration/gravity	S_a	1
Force	$S_F = S_E \times S_L{}^2$	1/16
Inertia mass	$S_M = S_F / S_a$	1/16
Time	$S_T = (S_L / S_a)^{0.5}$	0.5

bays primarily carry gravity loads. The seismic mass is taken as 235 kg/m^2, which is determined in consideration of the shake table's testing capacity. As a result, the total floor mass of each floor amounts to 144 t. For a one-bay MRF, the tributary floor mass amounts to 24 t. The prototype MRF is designed with a site classification of D located in Los Angeles, California, United States. The design of the prototype MRF follows the equivalent lateral force design method outlined in ASCE 7–16.[39] Relevant design parameters are listed in Table 1. The design fundamental period is estimated to be 0.44 s, and the design base shear is 480 kN, corresponding to a base shear of 80 kN for each MRF bay.

2.2 | Scaled tested frame

A 1/4-scale MRF was built for the shake table tests with consideration of the limitations on the physical size and testing capacity of the shake table located at The Hong Kong Polytechnic University. The scaling process of the prototype frame followed the principles of similitude, as detailed in Table 2. The tested frame's story height and bay width were scaled down to 1.2 and 1.6 m, respectively. Additionally, the floor mass of the tested frame was scaled to 1500 kg for each floor.

2.3 | SMAUD and SUD

Superelastic NiTi SMAUD specimens, which serve as the core components in the isolators, were provided by a commercial supplier in China. The manufacturer provided material information indicating an austenite finish temperature near 5°C, enabling the SMAUD specimens to demonstrate superelasticity at room temperature. Before the shake table tests, in-plane and out-of-plane cyclic tests on a pair of SMAUDs were conducted using an MTS machine. The dimensions of the tested SMAUDs specimens are shown in Figure 2B, and the corresponding cyclic behaviors are shown in Figure 2A, revealing its stable SC behavior as well as moderate energy dissipation capability during cyclic loading tests. For the in-plane behavior, the initial stiffness of a pair of tested SMAUDs is 455 kN/m, the phase transformation stiffness (similar to post-yield stiffness) is 34 kN/m, and the yielding strength is around 2.8 kN. For the out-of-plane behavior, the initial

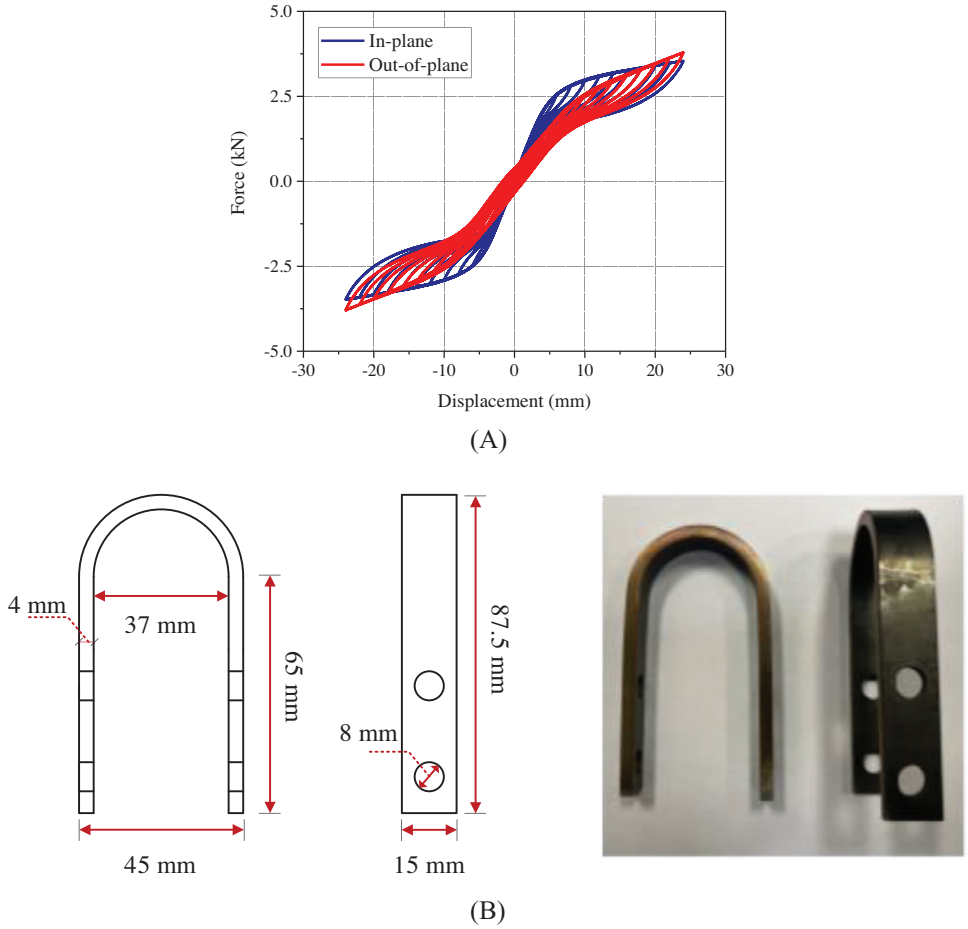

FIGURE 2 Superelastic SMAUD: (A) cyclic behavior and (B) tested specimens.

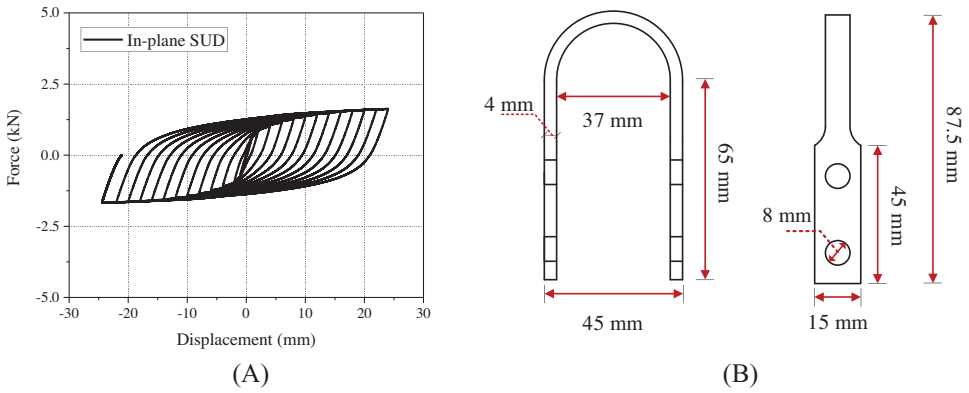

FIGURE 3 SUD: (A) cyclic behavior and (B) tested specimens.

stiffness is 233 kN/m, the post-yield stiffness is 79 kN/m, and the yielding strength is around 2.6 kN. The SMAUD specimens can restore their initial position without residual displacement when the loading displacement is up to 24 mm due to the excellent superelasticity of SMAs.

Additionally, an in-plane cyclic test on a pair of SUD specimens was also conducted for comparison. Figure 3A shows the corresponding cyclic behavior, and Figure 3B shows the dimensions of the tested SUD specimens. The initial stiffness of a pair of the tested SUDs is 682 kN/m, the post-yield stiffness is around 12 kN/m, and the yielding strength is around 1.4 kN. Compared with the SMAUD specimens, the hysteretic loops of SUDs were plumper, indicating more energy dissipation

capability. However, the residual displacement of SUDs was obvious and could accumulate with the increase of cyclic loading amplitude.

2.4 | Base isolators

Two types of base isolators were investigated in this paper, namely, (i) SMAUD-based isolators and (ii) SUD-based isolators. These isolators were tested by either installing or removing the critical components (SMAUDs or SUDs) within the isolators. Figure 4 demonstrates the configuration and components of the base isolator with SMAUDs and SUDs. The design method for the SMAUD-based isolators has been thoroughly documented in the previous study by Wang et al.[37] In this test, the isolator design was modified by replacing the rubber bearing with sliding surfaces with universal wheels to withstand vertical loads. Each isolator consists of four SMAUDs, multiple small-size universal wheels, four large-size universal wheels, and two supporting frames. Two supporting frames are fixed on the bottom cover plate of the isolator through high-strength steel bolts. Seven small-size universal wheels are mounted on each supporting frame. Four large-size universal wheels are mounted on the upper top cover plate of the isolator. The main design concept is to incorporate those specially designed universal wheels to support vertical loads, while their low friction has a minimal contribution to the horizontal load resistance. The combination of supporting frames and universal wheels can effectively restrict the vertical displacement of the isolator. Four SMAUDs are arranged symmetrically around the center. The SMAUDs are connected to the isolator through bolts, with their two straight segments affixed to the bottom and top steel cover plates. These SMAUDs serve as the critical lateral load-resistant components of the isolator, enabling SC and energy dissipation abilities via intrinsic flag-shaped hysteretic behavior under seismic loading. The working mechanism of the isolator subjected to horizontal relative displacement is shown in Figure 4A. Among the installed four SMAUDs, two SMAUDs exhibit rolling–bending mechanical behavior under in-plane loading, whereas the other two SMAUDs demonstrate torsion-bending behavior under out-of-plane loading.

For a comparison purpose, the configuration of a traditional base isolator with SUDs closely resembles that of the isolator with SMAUDs. To be compatible with the strength of the SMAUDs, the SUD is shaped with a semicircle with a narrow width of 8 mm connected by two straight parts with a width of 15 mm. The SUDs are made of Q235 steel with a yield stress of 235 MPa and Young's modulus of 2.1×10^5 MPa. The detailed dimensions of the SMAUDs and SUDs are shown in Figure 4B,C.

Before being mounted on the shake table, quasi-static cyclic tests of the isolators were performed using a customized loading system to examine their cyclic behavior. In the loading system, a hydraulic actuator is horizontally fixed on a supporting frame through high-strength bolts, as shown in Figure 5A. The load capacity of the hydraulic actuator is 20 t. The bottom cover plate of the isolator is fixed on the ground through four high-strength bolts. An H-beam is designed to facilitate the connection and transfer the horizontal load to the isolator: the bottom of the H beam is mounted on the upper cover plate of the isolator through bolts, and one end of the H beam is connected to the hydraulic actuator in the horizontal direction. Between the hydraulic cylinder and customized H beam, a circular load cell with a capacity of 3 t is used to measure the applied horizontal force. A displacement sensor is also installed in the horizontal direction to measure the relative horizontal displacement of the isolator. Figure 5B exhibits the deformed pattern of the isolator subjected to a horizontal load. Figure 5C shows the force-displacement relationship of the tested isolator, which displays the anticipated flag-shaped SC ability and stable energy dissipation. Figure 5C shows the initial stiffness of the SMAUD-based isolator is around 720 kN/m, and its post-yield stiffness is around 134 kN/m. The 'yielding' force is around 7 kN, and the corresponding "yielding" displacement is around 7 mm. The "yielding" behavior can reduce the lateral force to be transmitted to the superstructure. The energy dissipation is relatively smaller than traditional base isolators (e.g., lead rubber bearings). As suggested by Wang et al.,[37] the energy dissipation of the SMAUD-based isolators could be further enhanced by adding supplementary energy-dissipating elements, if necessary.

2.5 | Frame model

Figure 6 illustrates the overview of the scaled frame installed on the shake table for the test. The test was conducted on a 3 m × 3 m shake table at The Hong Kong Polytechnic University. The shake table can generate seismic excitation along a single direction and achieve a peak ground acceleration of ±1 g with a payload of 5 t. Two identical MRFs were built and tested: one equipped with SMAUD-based isolators and the other with SUD-based isolators. Figures 6 and 7A show that the

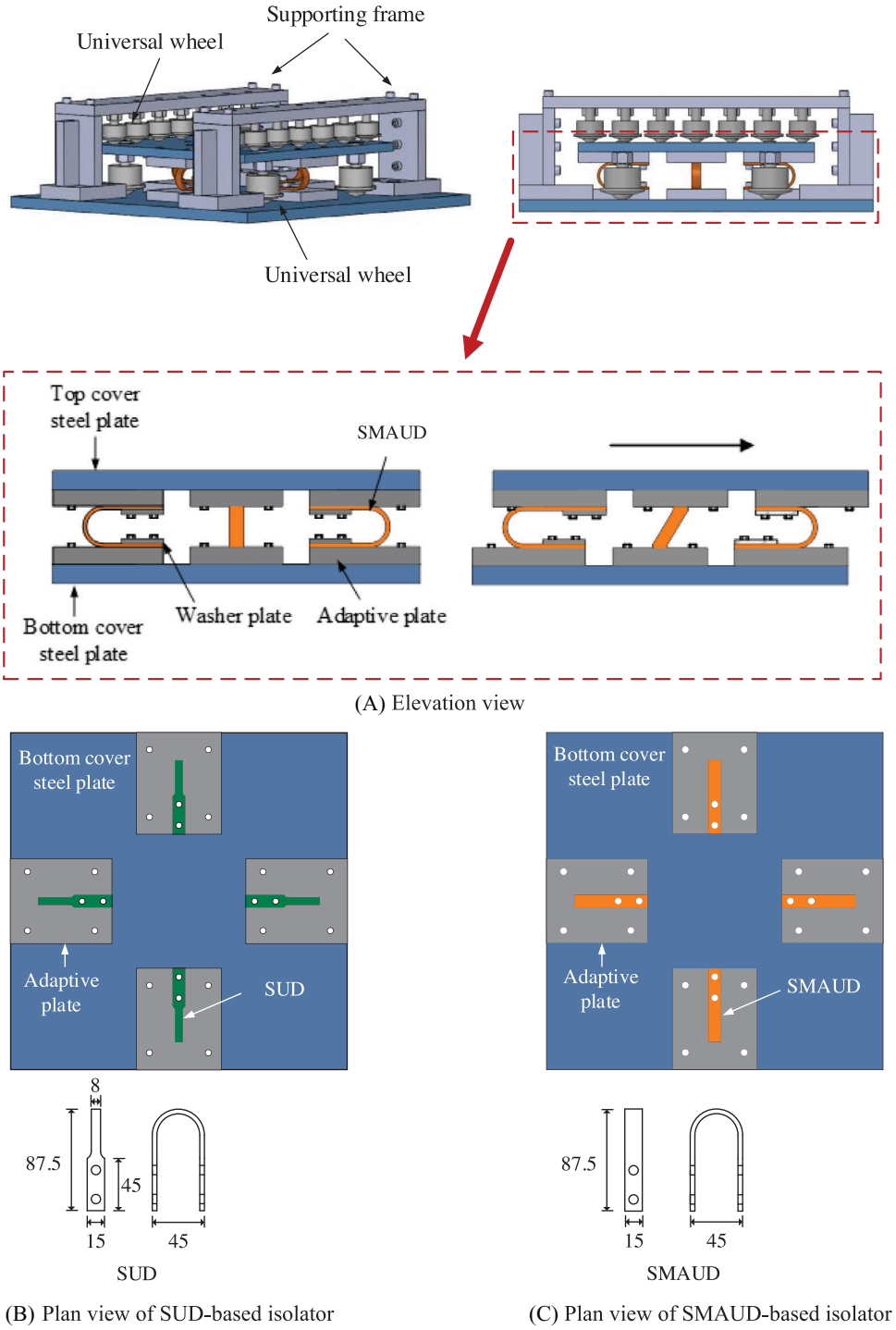

FIGURE 4 Design configurations of isolators.

test setup comprises three main components: the tested MRF with isolators, a mass simulation frame, and a supporting frame. The bottom steel cover plates of the isolators are fixed on the shake table, as shown in Figure 7C. Beams and columns with a built-up section of H80 × 50 × 4.5 are selected for the tested MRF. The selected section size is almost the smallest wide flange section available in the market, which is actually larger than that required according to the similitude law. All the beam–column connections are welded moment resisting connections. To enhance the structural integrity, a base beam is added to connect the two column bases of the MRF, with the column bases of the MRF fixed on the top flange of the base beam. In the connection zone, stiffeners are attached to the web of the base beam to prevent local buckling. The supporting frame is designed with sufficient stiffness to prevent the occurrence of out-of-plane deformation of the MRF throughout

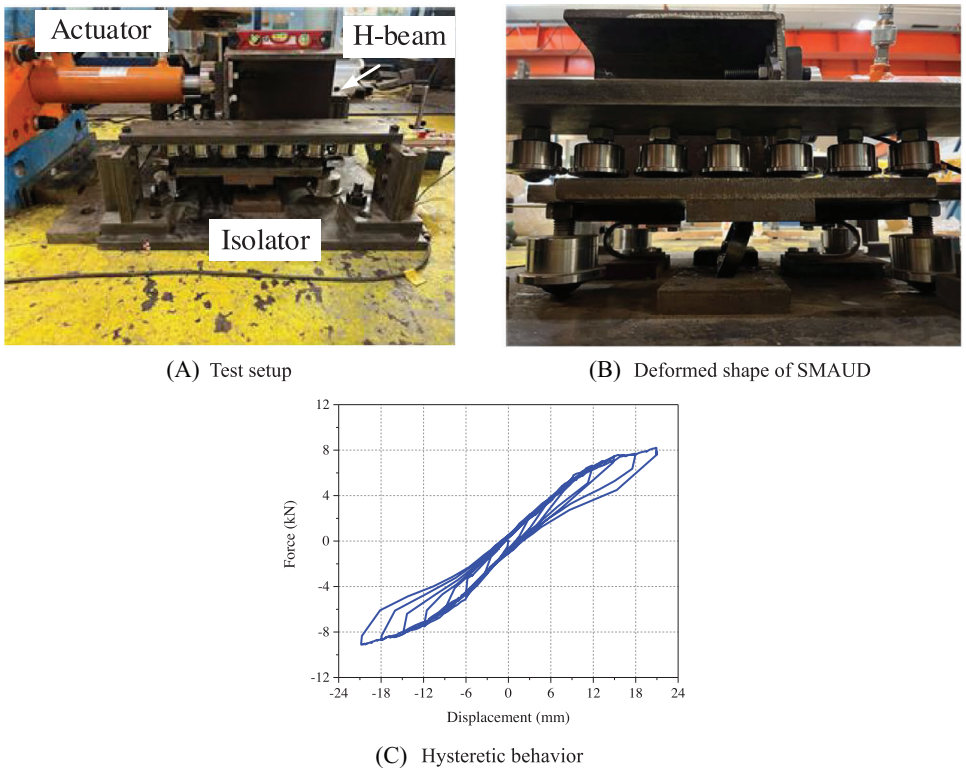

(A) Test setup (B) Deformed shape of SMAUD

(C) Hysteretic behavior

FIGURE 5 Cyclic tests of the SMAUD-based isolator.

the tests. Four rollers are installed between the supporting frame and tested MRF in each story to provide effective out-of-plane constraints whilst exerting minimal resistance to horizontal motion. Figure 7D demonstrates a detailed photo of a typical roller installed between the tested MRF and the supporting frame. The mass simulation frame comprises steel plates to simulate the horizontal frame mass. For each floor, 12 steel plates are used to simulate 1500 kg of seismic floor mass, and these plates are interconnected using steel bars. In particular, the top and bottom ends of the H-section columns in the mass simulation frame are connected to these plates and the shake table through hinge connections, as shown in Figure 7E. At each floor level, the mass simulation frame is connected to the tested MRF through a horizontal link with hinge connections at two ends, as shown in Figure 7B. This design enables free rotational movement and can only transmit horizontal forces to the tested MRF. In this manner, the mass simulation frame does not provide any horizontal stiffness or strength to the tested MRF, and it only bears vertical gravity loads and produces the P-Delta effect on the tested MRF. All beams and columns are made of Q235 steel with a yield stress of 235 MPa according to the Chinese code.

3 | EXPERIMENTAL PROGRAM

3.1 | Sensor system setup

Four laser displacement transducers (IL-300, Keyence, USA), six strain gauges (YFLA, Tokyo Measuring Instruments Lab, Japan), and six accelerometers (KD 1300) were installed. Figure 8 provides close-up views of several kinds of installed sensors, including a laser displacement transducer, a strain gauge, and an accelerometer. A reference steel subframe was built adjacent to the shake table to accommodate the installation of the required laser displacement sensors, which measured the absolute displacements of each floor and the upper cover plate of the isolator. One laser displacement transducer was installed on the edge of the shake table to measure the absolute displacement of the shake table. These laser displacement transducers enabled the close monitoring of the peak and residual displacements of the tested MRF and isolators following each test run. Furthermore, two accelerometers were installed on each floor to collect absolute floor acceleration data. Another accelerometer was installed on the upper cover plate of the isolator. Additionally, an extra accelerometer was installed on top of the shake table to measure the ground accelerations that the tested MRF experienced during

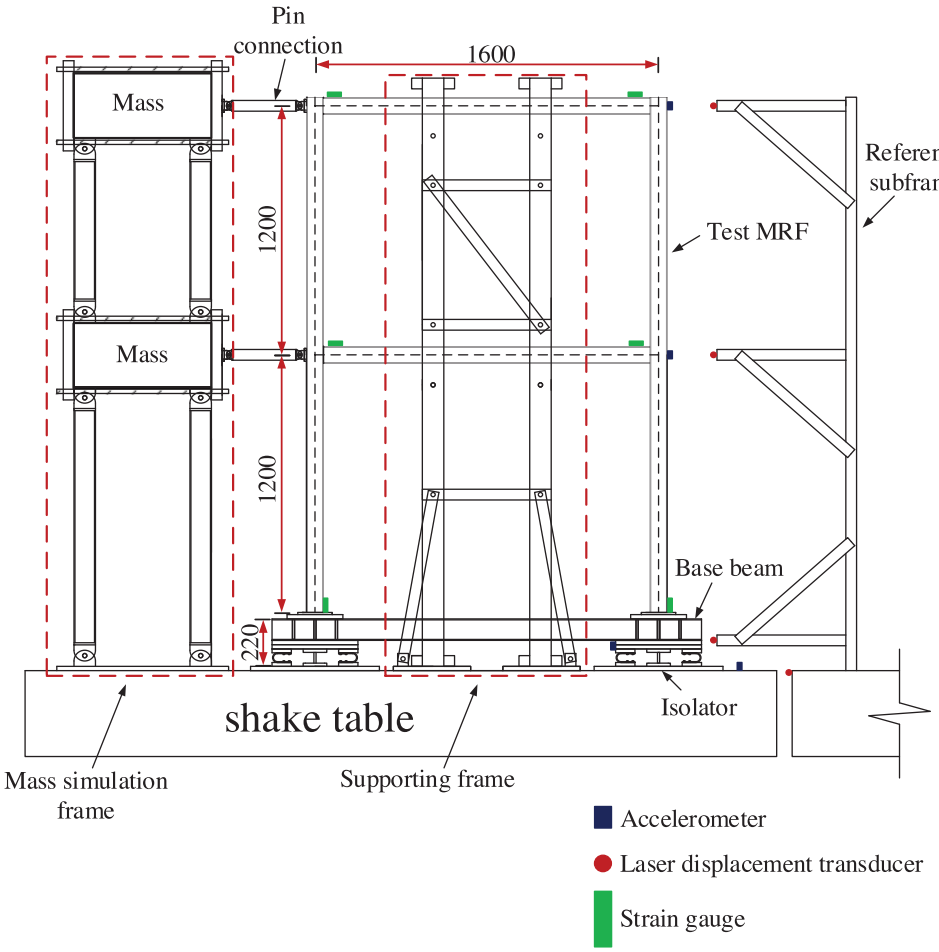

FIGURE 6 Elevation of the scaled frame model.

TABLE 3 Ground motion properties.

Seismic motion	Name and year	Recording station	Magnitude	PGA (g)	Type
LA17	Northridge, 1994	Sylmar	6.7	0.57	Far-field
NF09	Erzincan, 1992	95 Erzincan	6.7	0.43	Near-field

shake table tests. The collected ground accelerations were subsequently used as seismic excitations in the numerical analyses. Figure 6 shows the arrangement of the sensors. The test data generated by the laser displacement transducers, strain gauges, and accelerometers were collected by the data collection system (EDX-100A, KYOWA, Japan) at a sampling frequency of 1000 Hz.

3.2 | Selection of seismic motions

Before and after each formal test, white noise ground motion with small amplitude was applied as excitation to monitor changes in the natural frequency of the tested MRF, serving as an indicator of the structural condition of the MRF. In the formal tests, two ground motion records, denoted as LA17 and NF09, were selected as the input ground motions. Developed by Sommerville,[40] LA17 and NF09 represent far-field and near-field seismic ground motions, respectively. LA17 represents a design basis earthquake (DBE) level in Los Angeles. NF09 is a near-fault ground motion containing a considerable long-period component that may adversely affect traditional base isolated systems, leading to substantial isolation deformation and residual drift. The details of LA17 and NF09 are presented in Table 3. Based on the similitude law, the time scale of

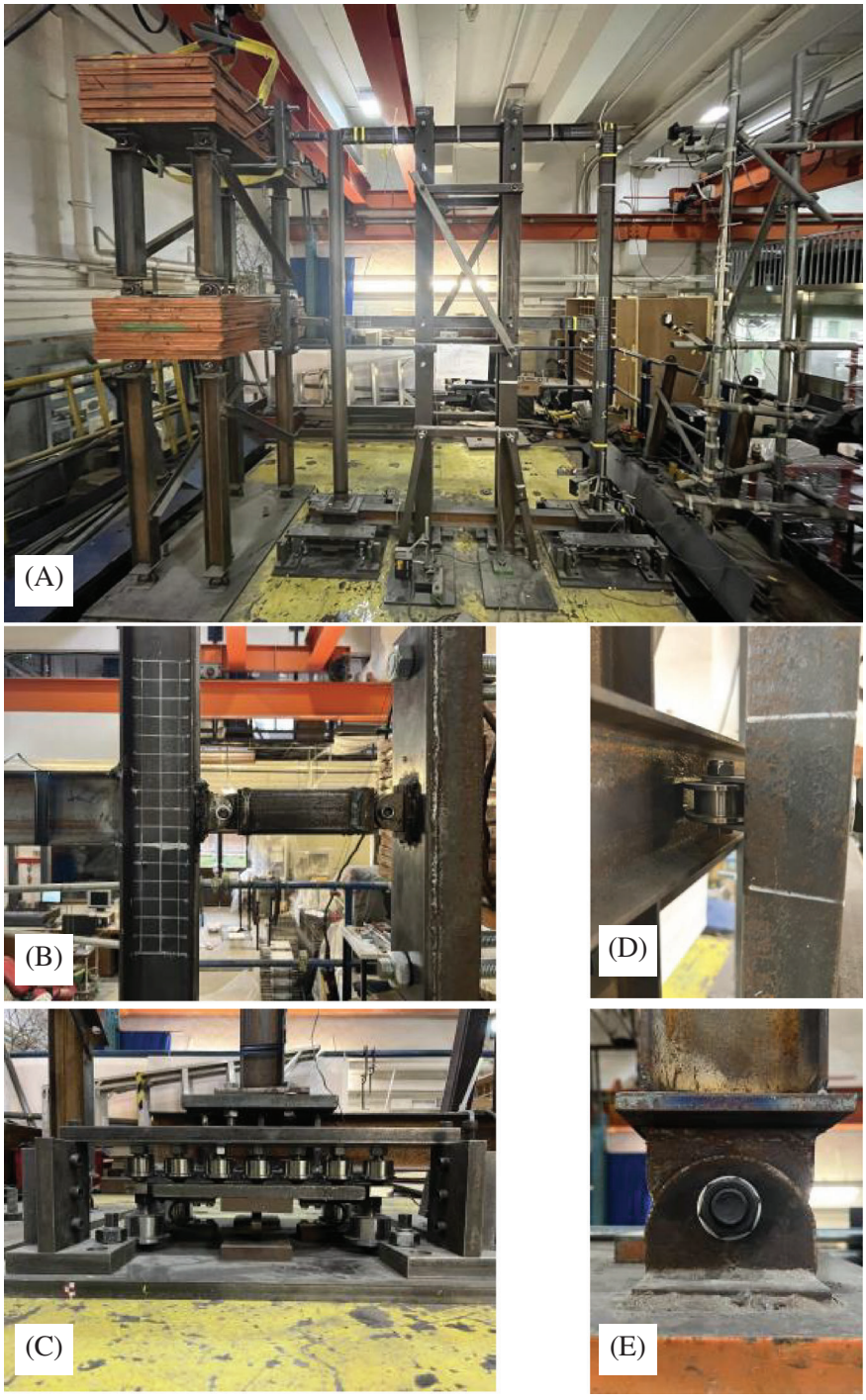

FIGURE 7 Experimental setup: (A) overview of the tested frame, (B) the link connecting the tested MRF with the mass simulation frame, (C) SMAUD-based isolator, (D) roller between the tested MRF and supporting frame, and (E) hinge connection at the column base of the mass simulation frame.

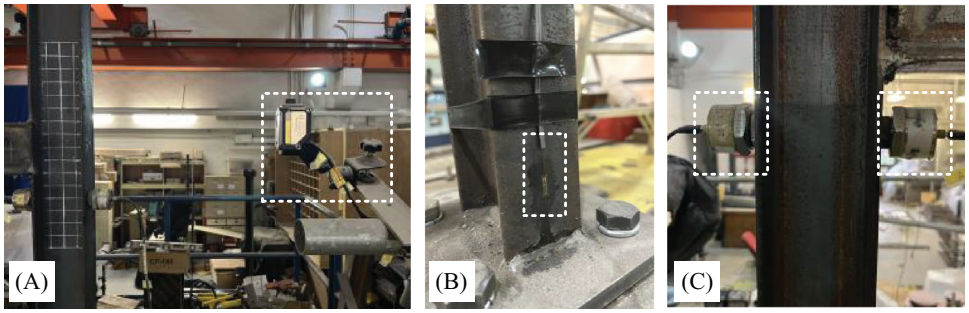

FIGURE 8 Installed sensors: (A) laser displacement transducer, (B) strain gauge, and (C) accelerometer.

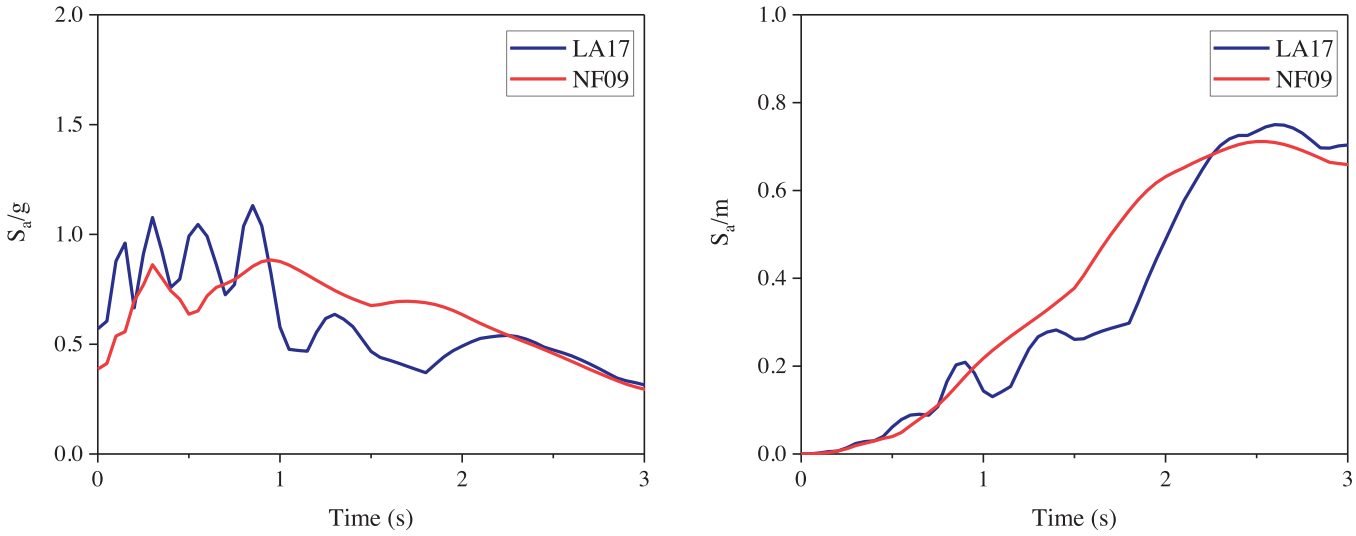

FIGURE 9 The elastic response spectrum of two input ground motion records (5% damping ratio).

TABLE 4 Loading sequences for the MRF with SMAUD-based isolators.

Test No.	Ground motion	Scale factor	PGA (g)
0r	Random excitation		
1	LA17	0.25	0.14
1r	Random excitation		
2	LA17	0.5	0.29
2r	Random excitation		
3	LA17	1.0	0.57
3r	Random excitation		
4	LA17	1.5	0.89
4r	Random excitation		
5	LA17	0.75	0.43
5r	Random excitation		
6	NF09	0.25	0.11
6r	Random excitation		
7	NF09	0.5	0.22
7r	Random excitation		
8	NF09	1.0	0.43
8r	Random excitation		
9	NF09	0.75	0.32
9r	Random excitation		

the ground motions was scaled down by a ratio of 0.5. The spectral acceleration and displacement of LA17 and NF09 are exhibited in Figure 9.

To investigate the seismic performance of the tested MRF with SMAUD-based isolators under various earthquake intensities, the peak ground accelerations (PGAs) of ground motions LA17 and NF09 were also scaled to different intensity levels and then employed as seismic excitation during the tests. The loading sequences of the ground motions in the formal tests are presented in Table 4. Nine seismic ground motion tests (denoted as Nos. 1–9) and ten random excitation tests (denoted as Nos. 0r–9r) were performed. Test 4 had the highest ground motion intensity with a PGA of 0.89 g, representing the maximum considered earthquake (MCE) level and simulating the mainshock. Following a random excitation test

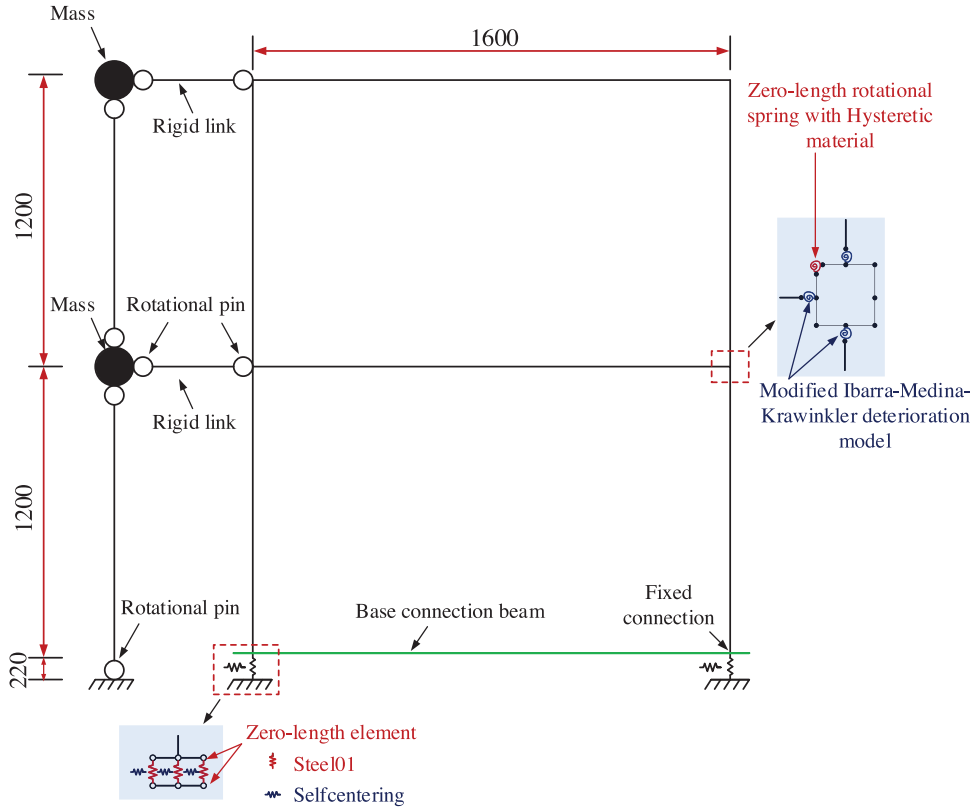

FIGURE 10 Numerical model of the tested MRF.

4r, one scaled-down LA17 ground motion with a PGA of 0.43 g was applied to investigate the seismic behavior of the MRF under the succeeding aftershock. Subsequently, NF09 ground motions were employed as seismic excitation to explore the behavior of the tested MRF under near-fault ground motions.

In contrast, the MRF with SUD-based isolators was only tested under two ground motions, namely LA17 × 1.0 and LA17 × 1.5, on the shake table, given the apparent accumulation of residual deformation observed in the experiments.

For the two tested MRFs with SMAUD-based and SUD-based isolators, no repairs or replacements were undertaken on the frame members or isolators throughout the entire shake table testing process, considering the associated technical difficulty in real-world scenarios.

4 | NUMERICAL SIMULATIONS

To compare with the experimental results, numerical simulations of the tested steel MRF were conducted using the finite element (FE) program OpenSees. Figure 10 shows the 2D FE model of the tested MRF. The model employs elastic beam–column elements to simulate the beams and columns of the tested MRF. Elastic beam–column elements are connected by zeroLength elements, where rotational springs are defined to simulate the nonlinear behavior of the plastic hinges at the connections. The plastic behavior of the beam-to-column connections is modeled using the modified Ibarra–Medina–Krawinkler model. The strength and stiffness deterioration are considered through relevant parameters based on the previous research.[41] The model also accounts for shear deformation in the panel zones of beam-column connections based on the research conducted by Gupta and Krawinkler.[42] In the numerical model, columns are fixed on the base connection beam. The base connection beam, in turn, is fixed on the top of the base isolators. Due to the limitations imposed by the supporting frame, only the in-plane behavior of the 2D frame is considered. To ensure the mass simulation frame does not contribute any horizontal stiffness to the MRF, it is modeled using leaning columns pinned at the base and interconnected through zeroLength rotational spring elements with minimal stiffness. At each floor, the lateral displacement of the mass simulation frame is set to be the same as that of tested MRF through rigid links. Consequently, the dynamic simulations

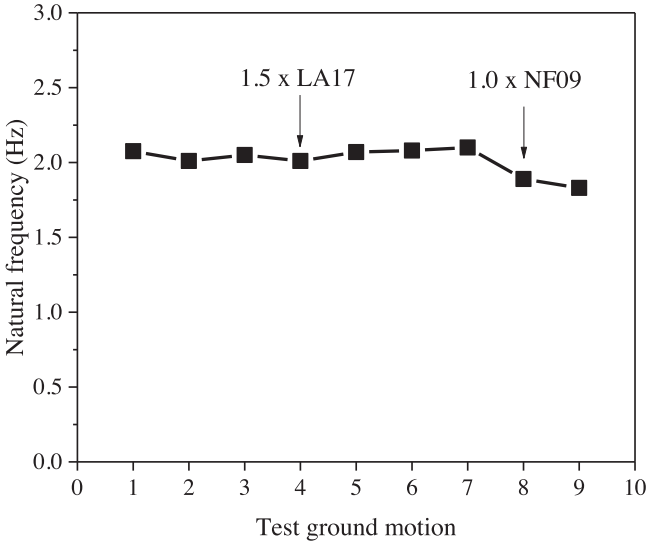

FIGURE 11 Changes in the natural frequency of the MRF with SMAUD-based isolators during shake table tests.

account for the P-Delta effect. The actual acceleration data collected by the accelerometer installed on the shake table are applied as seismic excitation in the numerical simulations.

To accurately capture the isolator behavior under ground motions, the SMAUD-based isolators are modeled through multiple zeroLength elements in OpenSees (as shown in Figure 10), where the horizontal elements use the *SelfCentering* material to capture the flag-shaped hysteretic behavior of SMAUDs in the horizontal direction, and the vertical elements use the *Steel01* material to simulate the vertical and rotational stiffness of the isolator. The key properties of the *SelfCentering* material include initial stiffness, post-yield stiffness, yielding force, and hysteresis loop width parameter. The required *Steel01* material properties were determined based on the cyclic test results of isolators in Section 2.4, as well as the natural frequency identified in the random excitation tests. A damping ratio of 6% was adopted in the numerical simulation to consider the inherent damping of the whole isolated frame.

Another steel MRF with fixed bases was also numerically modeled and simulated for comparison. The design details of the MRF were the same as those of the aforementioned MRF model, except that fixed bases replaced the isolators. The numerical simulation results of the two MRFs are compared in Section 5.5.

5 | EXPERIMENTAL AND NUMERICAL RESULTS

5.1 | Natural frequency

Before the normal test, the natural frequency of the tested MRF with SMAUD-based isolators was identified through the white noise excitation with PGA of 0.02 g. The identified natural frequency of 2.07 Hz closely matched the estimated frequency in the design stage. Before and after each seismic ground motion input, white noise random excitations were applied again to monitor the variance of the natural frequencies of the tested MRF. The changes in the natural frequency throughout the whole shake table test process are shown in Figure 11. The natural frequency of the tested MRF remains relatively stable until ground motion No. 7, implying that almost no damage occurs in the tested MRF during the substantial ground motion LA17 × 1.5. After ground motion No. 7, a slight decrease in the natural frequency is observed, which can be due to two possible reasons: (1) accumulation of minute structural damage and (2) decreased vertical stiffness of the isolator.

5.2 | Frame response

Figure 12 compares the time histories of the roof displacement between the test and numerical responses in all the experimental cases with different PGAs. These figures are arranged in ascending order according to the intensity levels of the ground motions. The experimental peak roof displacement is around 15 mm under the test case of LA17 × 0.5 and increases

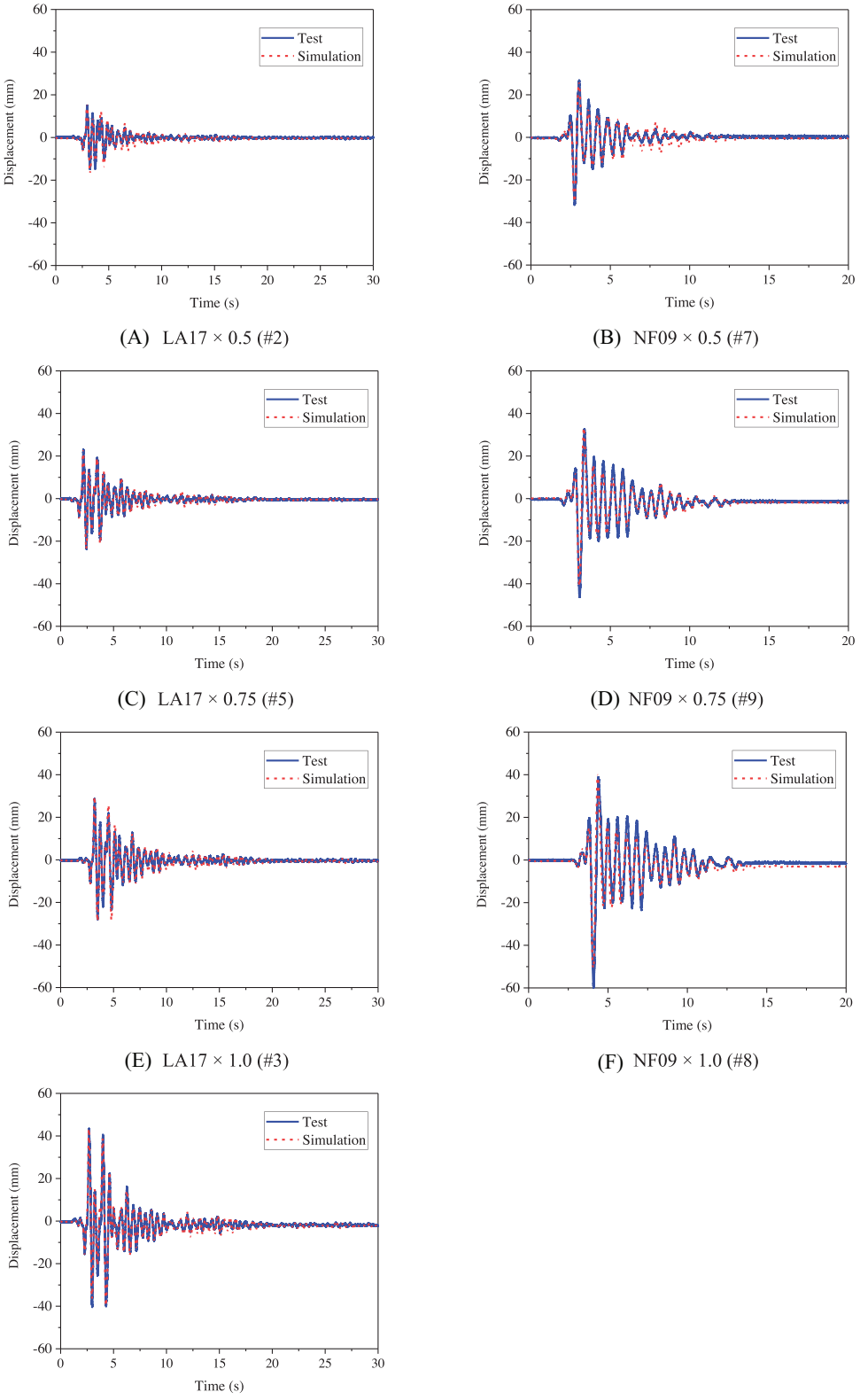

FIGURE 12 Time histories of the roof displacement of the MRF with SMAUD-based isolators under LA17 and NF09 with various seismic intensities.

TABLE 5 Comparison of peak values between experimental and numerical results of the MRF with SMAUD-based isolators.

Ground motion	Inter-story drift ratio				Acceleration				Isolator displacement	
	Test		Simulation		Test		Simulation			
	1st story	2nd story	1st story	2nd story	1st story	2nd story	1st story	2nd story	Test	Simulation
LA17 × 0.5	0.83%	0.55%	0.74%	0.54%	0.27 g	0.34 g	0.23 g	0.29 g	2.34 mm	4.67 mm
LA17 × 0.75	1.17%	0.79%	1.04%	0.79%	0.35 g	0.53 g	0.33 g	0.53 g	6.40 mm	6.58 mm
LA17 × 1.0	1.39%	1.04%	1.27%	1.03%	0.43 g	0.74 g	0.43 g	0.67 g	7.25 mm	8.15 mm
LA17 × 1.5	2.12%	1.53%	1.79%	1.50%	0.59 g	0.86 g	0.63 g	0.89 g	13.89 mm	12.78 mm
NF09 × 0.5	1.60%	1.03%	1.32%	0.95%	0.41 g	0.60 g	0.39 g	0.54 g	9.36 mm	8.13 mm
NF09 × 0.75	2.27%	1.57%	1.79%	1.31%	0.51 g	0.72 g	0.52 g	0.72 g	15.76 mm	12.55 mm
NF09 × 1.0	3.01%	1.98%	2.26%	1.55%	0.63 g	0.91 g	0.69 g	0.92 g	21.60 mm	20.24 mm

to about 28 and 43 mm under the test cases of LA17 × 1.0 and LA17 × 1.5, respectively. In the test case of near-fault ground motion (i.e., NF09 × 1.0), the peak roof displacement reaches about 59 mm. The experimental and numerical results exhibit a remarkable level of agreement, demonstrating the accuracy of the numerical model in predicting the peak roof displacement responses. Implementing SMA isolators with stable SC performance and energy dissipation effectively prevents residual displacement in the frame during the shake table tests, even under a ground motion with a high-intensity level, for example, LA17 × 1.5. This result indicates the tested MRF equipped with SMAUD-based isolators exhibits exceptional seismic resilience against MCE ground motions with negligible residual deformation, which will substantially reduce post-earthquake repair expenses and downtime. To evaluate the influence of aftershocks, additional test cases were conducted using the scaled-down versions of ground motions (i.e., LA17 × 0.75 and NF09 × 0.75) after the tests of LA17 × 1.5 and NF09 × 1.0. Notably, no repairs or replacements were undertaken on the frame or isolators throughout the entire shake table testing process. The roof displacement time histories recorded during LA17 × 0.75 and NF09 × 0.75 show no residual deformation, indicating the robustness of the tested MRF in withstanding the mainshock and subsequent multiple aftershocks without additional repair measures.

Figure 13 shows the time histories of inter-story drift ratios in the test cases of LA17 × 1.0, LA17 × 1.5, and NF09 × 1.0, corresponding to the DBE, MCE, and near-fault ground motions, respectively. The inter-story drift ratios are determined by calculating the relative displacements between adjacent floors measured by laser displacement transducers. The maximum drift ratios of the tested MRF under the DBE and MCE levels are approximately 1.39% and 2.12%, respectively; for the NF09 × 1.0, the maximum drift ratio is 3.01%. At the end of all test cases, no evident residual inter-story drifts are observed. The corresponding inter-story drift time histories obtained from the numerical analyses matched the shake table test results. This agreement validates the effectiveness of the numerical model developed. The peak drift values for all test cases and simulations are summarized in Table 5. The reason that relatively large peak inter-story drifts are observed in the tested frame without evident residual inter-story drifts could be due to the effect of upper plate rotation, which is further discussed in Section 5.4. Figure 14 shows the time histories of the absolute accelerations for the first and second stories of the tested MRF in three different cases: LA17 × 1.0, LA17 × 1.5, and NF09 × 1.0, where the experimental and numerical results are also compared. In the LA17 × 1.0 case, the peak absolute acceleration values were recorded as 0.43 and 0.74 g for the first and second floors, respectively. When subjected to LA17 × 1.5, the peak absolute acceleration values rise to 0.59 and 0.86 g for the first and second floors, respectively. In the NF09 × 1.0 case, the peak absolute acceleration values are 0.63 and 0.91 g for the first and second floors, respectively.

Figure 15 shows the final state of a beam–column connection with no evident damage after all shake table tests. Figure 16 shows the strain time histories measured by three strain gauges mounted on the test MRF in the LA17 × 1.5 case. SG1 and SG2 are two strain gauges mounted on the ends of the beam in the first story. SG6 is the strain gauge mounted on the column base. All the measured strain levels were below the yield strain of the steel material, indicating the beams and columns remained elastic under this ground motion. This is consistent with the observation in Figure 11: After the test of LA 17 × 1.5, no noticeable decrease in the natural frequency was observed, implying that the tested MRF with SMAUD-based isolators could withstand a strong earthquake with stable performance. After the whole series of seismic ground motions, the frequency of the MRF was identified as 1.83 Hz, about 89% of the initial frequency of about 2.07 Hz. The frequency reduction was attributed to two factors: the accumulation of minor damage in the frame and the partial loss of the rotational and vertical stiffness of the isolators due to the loosening of universal wheels. In fact, the frequency drop of the MRF was partially recovered by re-tightening the universal wheels after the completion of all the tests.

Figure 17 shows the time histories of the relative horizontal displacement of the SMAUD-based isolator obtained under four ground motions, namely LA17 × 1.0, LA17 × 1.5, NF09 × 1.0, and NF09 × 0.75, wherein the experimental and

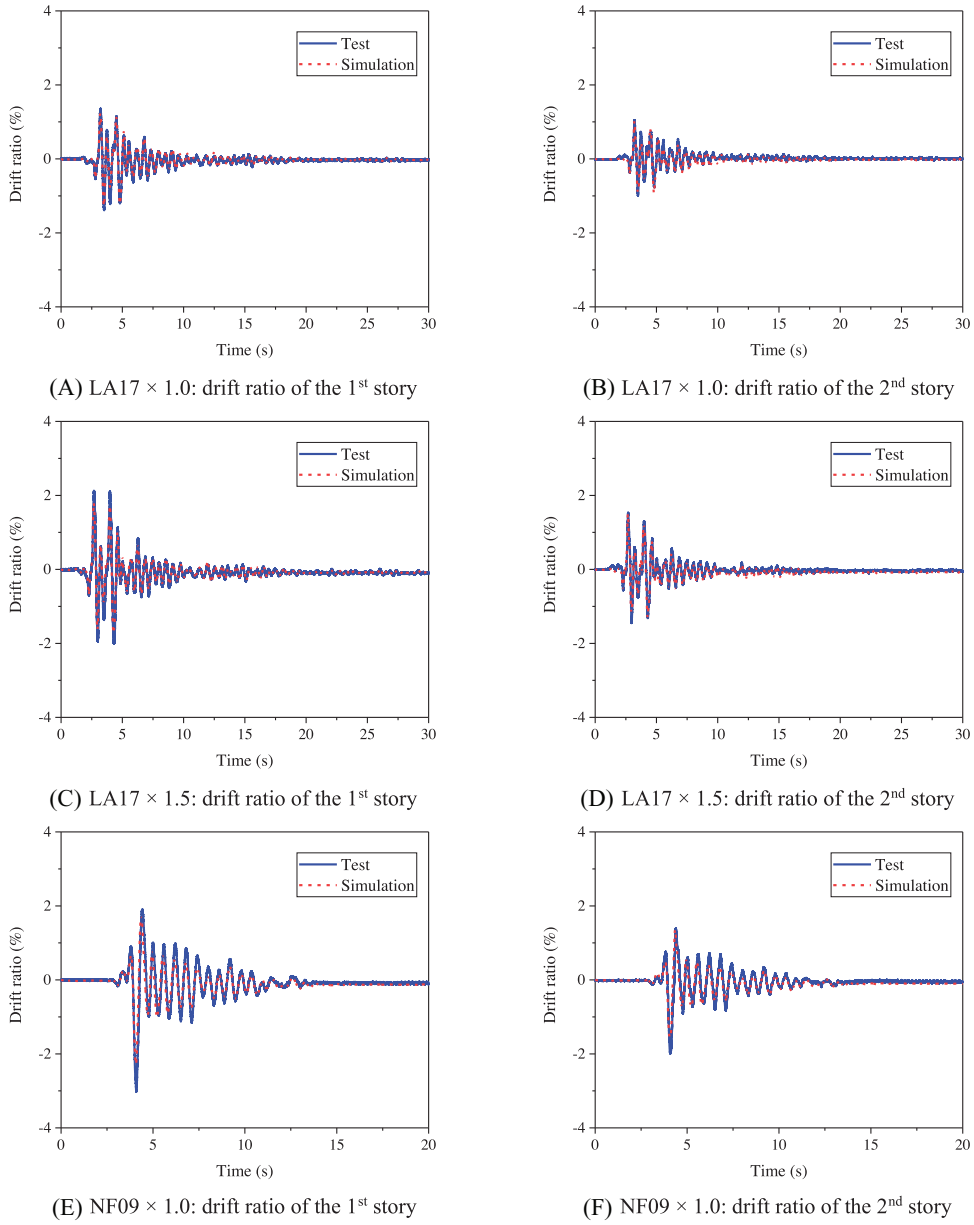

(A) LA17 × 1.0: drift ratio of the 1st story

(B) LA17 × 1.0: drift ratio of the 2nd story

(C) LA17 × 1.5: drift ratio of the 1st story

(D) LA17 × 1.5: drift ratio of the 2nd story

(E) NF09 × 1.0: drift ratio of the 1st story

(F) NF09 × 1.0: drift ratio of the 2nd story

FIGURE 13 Time history of inter-story drift ratios of the MRF with SMAUD-based isolators under LA17 and NF09 at various seismic intensities.

numerical results show good agreement again. In the LA17 × 1.5 case, the peak relative displacement of the isolator was 13.8 mm, higher than the "yielding" displacement of 7 mm obtained in Figure 5C. This result means the SMAUDs in the isolator entered the phase transformation stage from austenite to martensite. Amongst all test cases, the maximum relative displacement 21.4 mm was obtained in the near-fault case of NF09 × 1.0. This observation is consistent with the previous conclusion that near-fault ground motions with long-period components tend to cause substantial deformation in the isolators. No residual deformation was noted in the relative displacement of the isolators under all test cases, demonstrating the superior SC ability of the SMAUD-based isolator during mainshock and subsequent aftershocks.

5.3 | SMAUD-based isolators versus SUD-based isolators

To compare the seismic responses of different isolation systems, shake table tests were also conducted to examine the seismic responses of the MRF with SUD-based isolators under LA17 × 1.0 and LA17 × 1.5 ground motions. Figure 18

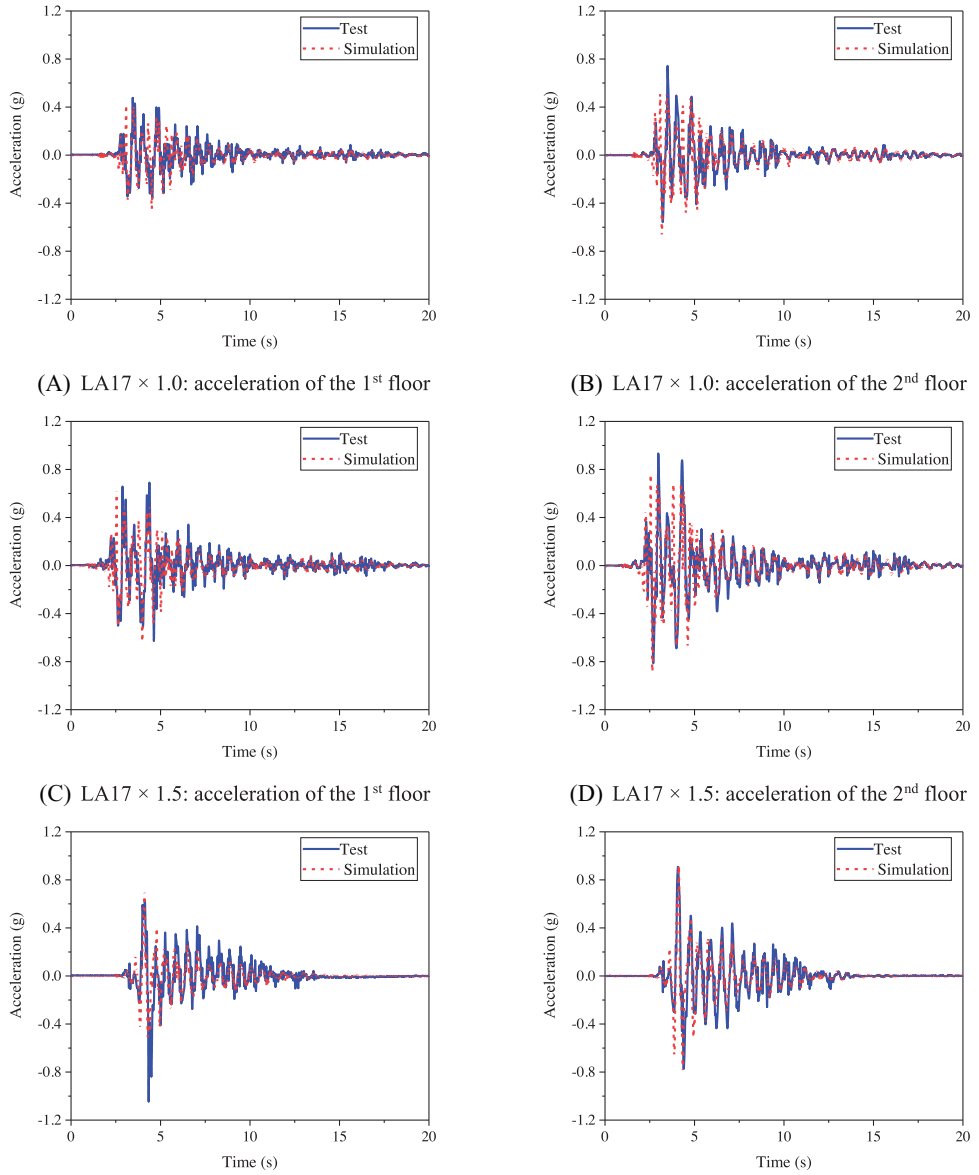

(A) LA17 × 1.0: acceleration of the 1st floor

(B) LA17 × 1.0: acceleration of the 2nd floor

(C) LA17 × 1.5: acceleration of the 1st floor

(D) LA17 × 1.5: acceleration of the 2nd floor

(E) NF09 × 1.0: acceleration of the 1st floor

(F) NF09 × 1.0: acceleration of the 2nd floor

FIGURE 14 Time history of absolute floor accelerations of the MRF with SMAUD-based isolators under LA17 and NF09 at various seismic intensities.

compares the responses of two tested MRFs equipped with SMAUD-based isolators and SUD-based isolators under LA17 × 1.0. The two MRFs exhibited similar frame responses, including inter-story drift ratios and roof displacements. For example, the peak roof displacements of the MRFs with SMAUD-isolators and SUD-isolators were 28.7 and 26.7 mm, respectively. The peak inter-story drift ratios with SMAUD-isolators and SUD-isolators were 1.39% and 1.37%, respectively. In the isolators, the peak relative displacement of the SUD-based isolator was 16.9 mm, considerably larger than 7.2 mm of the SMAUD-based isolator.

Figure 19 shows that under the ground motion of LA17 × 1.5, the peak roof displacements of two MRFs with SMAUD-isolators and with SUD-isolators were 43.5 and 35.7 mm, respectively. The peak inter-story drift ratios of the MRFs with SMAUD-isolators and with SUD-isolators are 2.12% and 2.00%, respectively. In general, the peak dynamic response of the MRF with SMAUD-based isolators is relatively larger than that with traditional SUD-based isolators. This was mainly caused by the lower yield strength of the SUD-based isolators, compared with the SMAUD isolators. However, the SUD-based isolator experienced a peak relative displacement of 41.9 mm, leading to a noticeable residual displacement of 11 mm

FIGURE 15 Final state of the beam-column connection in the MRF with SMAUD-based isolators.

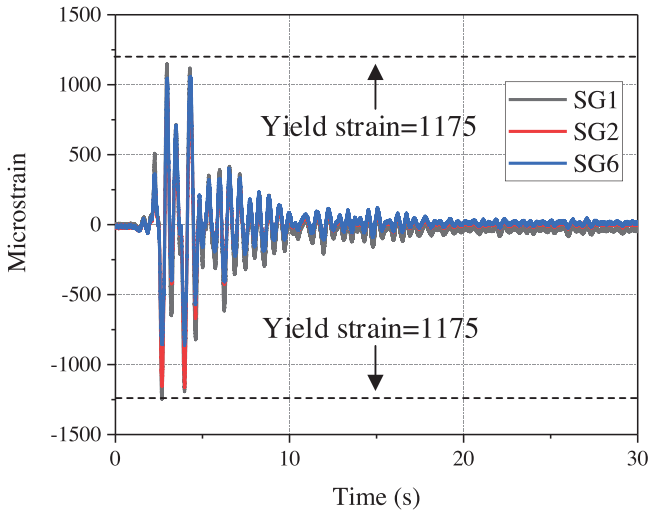

FIGURE 16 Time history of strain data of the MRF with SMAUD-based isolators measured during LA17 × 1.5.

at the end of the ground motion. By contrast, the peak relative displacement of the SMAUD-based isolator was 15.2 mm and exhibited a nearly zero residual displacement under the same seismic motion, demonstrating its excellent SC ability.

Furthermore, Figure 20 shows the final state of SUDs and SMAUDs taken out from the isolators after all the shake table tests. Evident in-plane residual deformation of about 11 mm was observed in the SUDs, which was about 26% of the peak relative displacement of 41.9 mm shown in Figure 19D. By contrast, no noticeable residual deformation was observed in the SMAUDs.

5.4 | Effect of upper plate rotation of isolators

The tested isolators experienced upper plate rotation due to the bending moment transmitted from the column bases during the shake table tests, as shown in Figure 21. As a result, it was observed that the behavior of the isolator upper plate combined rotation and horizontal movement. Such coupled behaviors of isolators were also discussed by other

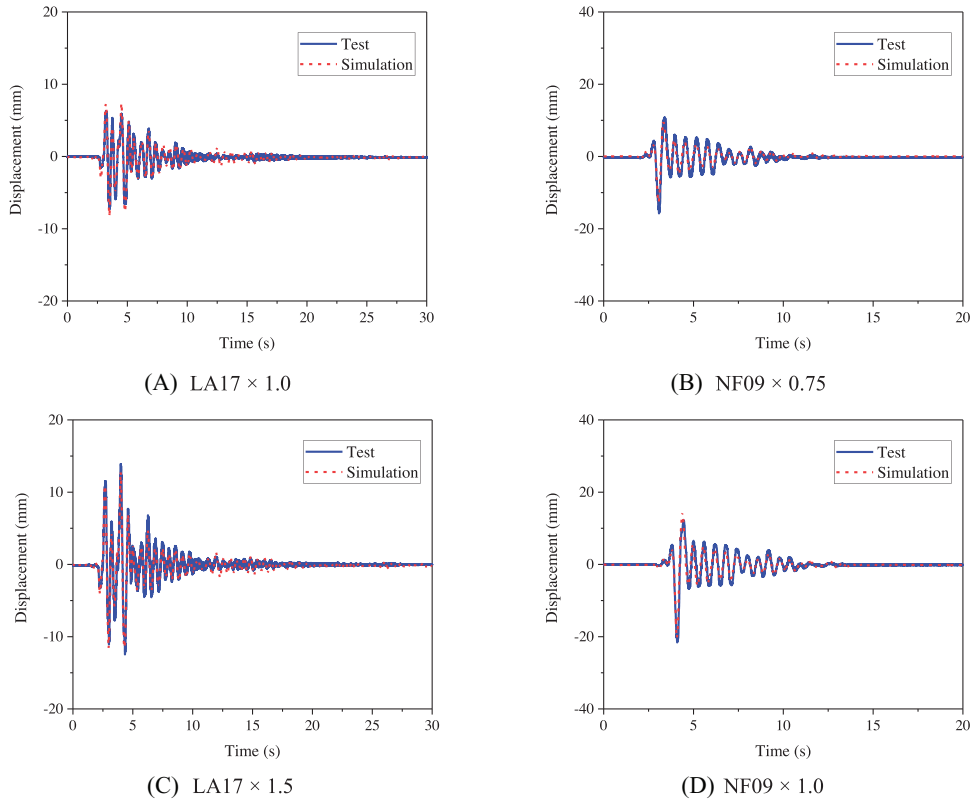

FIGURE 17 Time histories of the relative displacements of the SMAUD-based isolators under LA17 and NF09 at various seismic intensities.

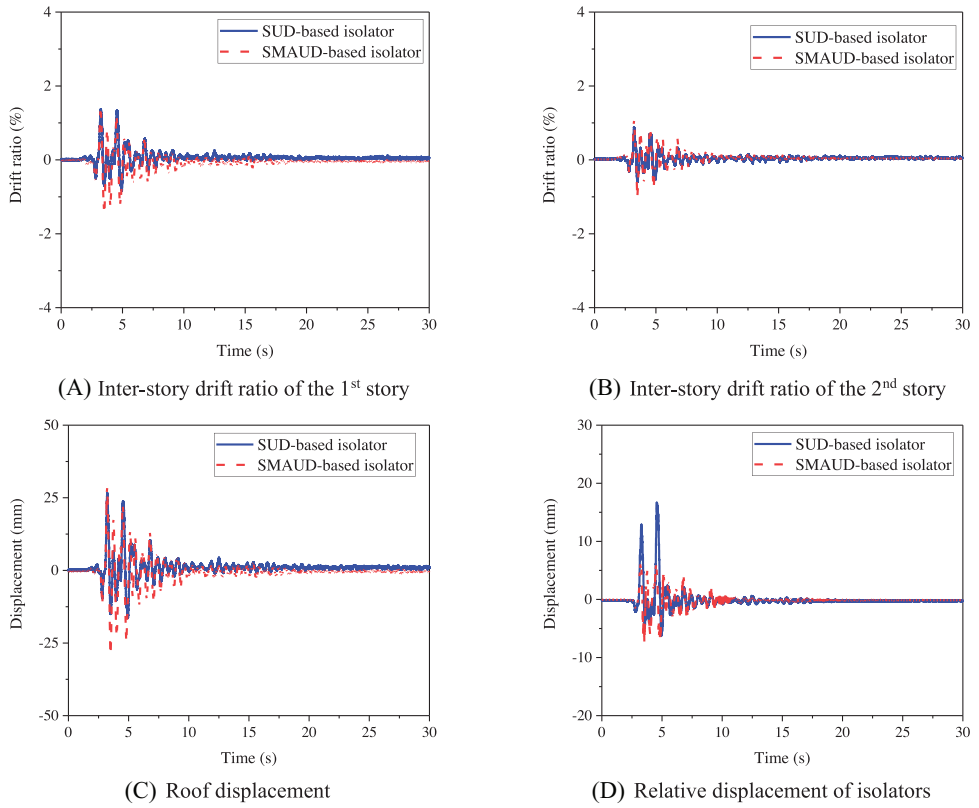

FIGURE 18 Comparison of the response of the MRFs with SMAUD-based isolators and with SUD-based isolators subjected to LA17 × 1.0.

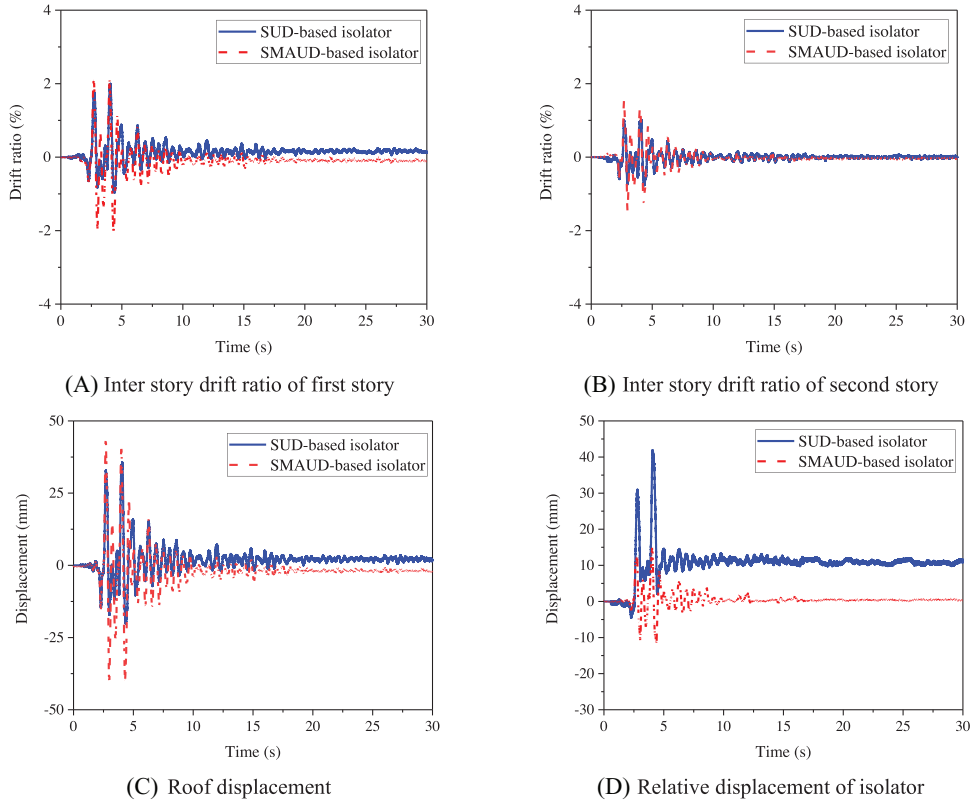

FIGURE 19 Comparison of response of MRFs with SMAUD-based isolators and with SUD-based isolators subjected to LA17 × 1.5.

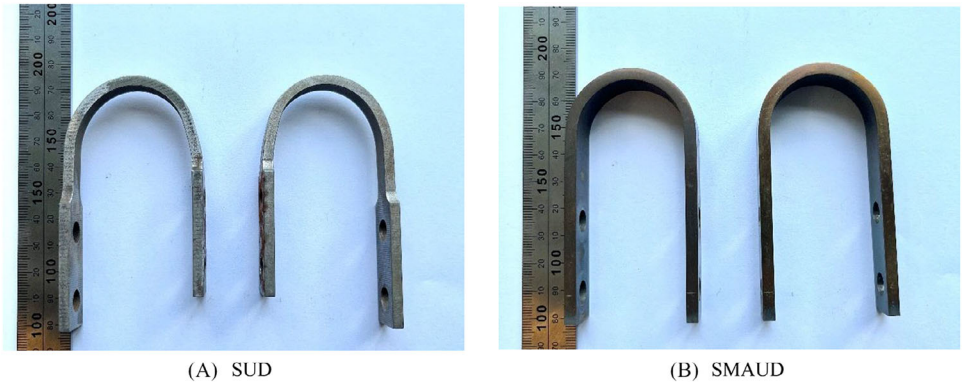

FIGURE 20 Final state of SUD and SMAUD specimens.

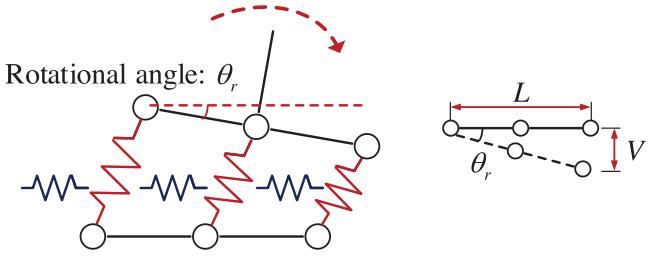

FIGURE 21 Upper plate rotation of isolator.

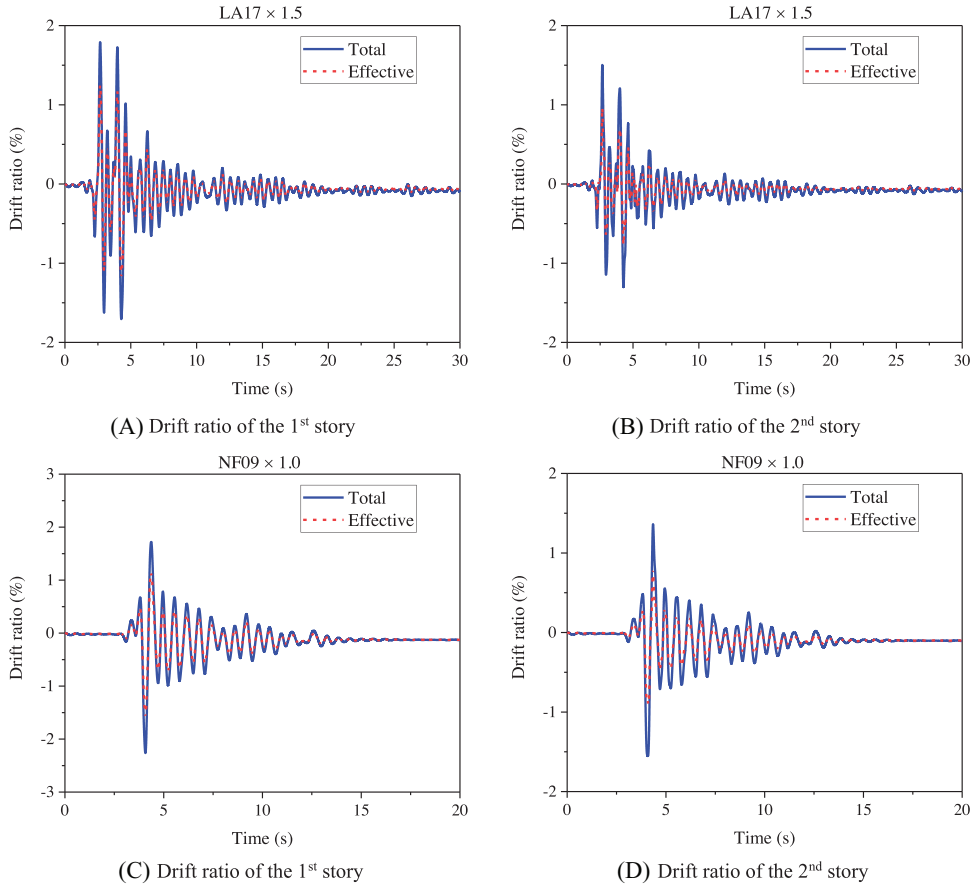

FIGURE 22 Comparison of nominal drift ratio and actual drift ratio in numerical simulations of the MRF with SMAUD-based isolators.

researchers.[43,44] The rotation of the upper plate of the isolators could lead to the rigid-body rotation of the tested MRF. Consequently, the measured inter-story drift response of the frame consists of two parts: the translational deformation part and the rigid-body rotation deformation part. The former is referred to as the effective inter-story drift because the latter is due to the isolator rotation instead of the frame deformation and thus will not cause damage to the frame members. The rotation angle of the isolator, θ_r, can be calculated as follows:

$$\theta_r = \frac{L}{V}, \tag{1}$$

where L is the width of the upper plate of the isolator, and V is the relative vertical displacement of the isolator.

Figure 22 compares the total and effective inter-story drift ratios in the numerical simulations of the cases of LA17 × 1.5 and NF09 × 1.0. The total inter-story drift ratio was determined by directly measuring the relative horizontal displacement between two adjacent floors and dividing it by the story height. The effective inter-story drift ratio was obtained by subtracting the isolator rotation from the total inter-story drift ratio. The isolator rotation-induced inter-story drift ratio contributed to a certain proportion of the overall frame response. As a result, the effective inter-story drift ratio could be considerably smaller than the total inter-story drift ratio. For example, in the test case of LA17 × 1.5, the peak values of total inter-story drift ratios were 1.79% and 1.50% in the first and second stories, respectively. By contrast, the peak values of effective inter-story drift ratios were only 1.25% and 1.10% in the first and second stories. In the test case of NF09 × 1.0, the maximum values of total inter-story drift ratios were 2.26% and 1.55% in the first and second stories, respectively. By contrast, the peak values of effective inter-story drift ratios were 1.55% and 0.88% for the first and second stories, respectively. The rotations of the isolator top plates explain why the frame remained elastic even when the inter-story drift ratio exceeded 3.0%. Such isolator rotations were mainly due to the low rotational and vertical stiffness of the isolators provided by those universal wheels. The isolator design needs to be improved to mitigate such rotations of the isolator top plates, which are undesirable during earthquakes.

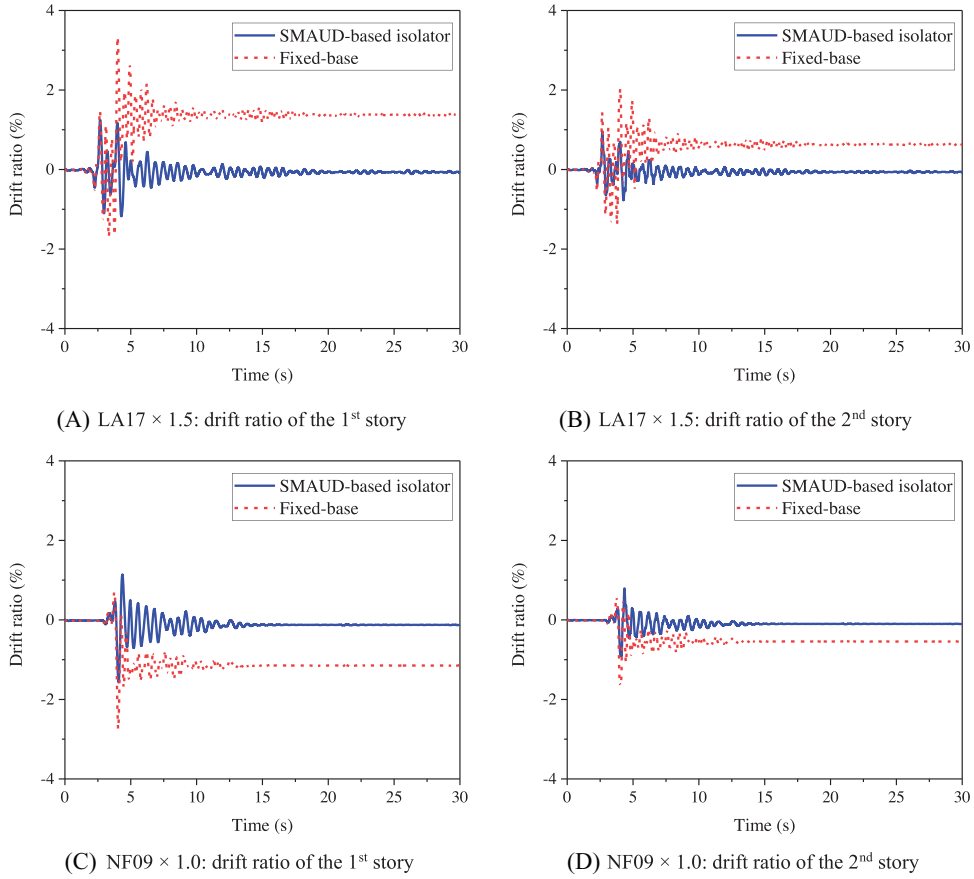

FIGURE 23 Comparison of effective inter-story drift ratios of the MRFs with fixed bases and with SMAUD-based isolators.

5.5 | SMAUD-based isolators versus fixed bases

This subsection compares the numerical simulation results of the two MRFs with SMAUD-based isolators and fixed bases individually, as the latter was not experimentally tested on the shake table. The natural frequencies of the two MRFs with SMAUD-based isolators and fixed bases were 2.07 and 2.68 Hz, respectively. Figure 23 compares the time histories of the inter-story drift ratios of the two MRFs under two ground motions, namely LA17 × 1.5 and NF09 × 1.0, wherein effective inter-story drift ratios of the MRF with SMAUD-based isolators are used. Under LA17 × 1.5, the peak inter-story drift ratios of the MRFs with SMAUD-based isolators and fixed bases were 1.25% and 3.32%, respectively. Moreover, obvious residual inter-story drift ratios were observed in the first and second stories of the MRF with fixed bases, which were 1.37% and 0.63%, respectively. Under NF09 × 1.0, the peak inter-story drift ratios of the MRFs with SMAUD-based isolators and fixed bases were 1.55% and 2.73%, respectively. Similarly, obvious residual inter-story drift ratios were observed in the first and second stories of MRFs with fixed bases, which were 1.15% and 0.54%, respectively. In general, peak and residual inter-story drift ratios of the MRF with SMAUD-based isolators were smaller than those of the MRF with fixed bases, confirming the effectiveness of the SMAUD-based isolators.

6 | DISCUSSIONS

Based on the experimental and numerical results presented in this section, the tested isolator design combining SMAUDs and slide surface needs to be meticulously improved in future studies in consideration of the following aspects:

(1) The low rotational stiffness of the SMAUD-based isolators, which caused undesirable upper plate rotation of the isolators, needs to be increased;

(2) Despite their superior SC capability, the energy dissipation of the SMAUD-based isolators is relatively small and needs to be further enhanced;
(3) The long-term reliability of the SMAUD-based isolators should be further examined, considering that the potential wearing and freezing of universal wheels may cause deviations from the expected behavior and performance of the sliding surface.

Improved isolator designs that integrate SMAUDs with traditional laminated rubber bearings, which can provide sufficient vertical and rotational stiffness, and supplementary energy dissipators (such as SUDs and lead cores) will be explored to achieve the enhanced performance of the SMAUD-based seismic base isolators.

7 | CONCLUSIONS

A steel MRF equipped with novel SMAUD-based isolators was proposed and investigated experimentally and numerically. The seismic resilient performance of the isolated MRF was studied by conducting a series of uni-directional shake table tests on a 1/4-scale model of a two-story, one-bay steel MRF subjected to ground motions of different intensities levels. The major conclusions can be summarized as follows:

(1) The SMAUD-based isolators exhibited stable, excellent SC ability and moderate energy dissipation under nine consecutive ground motions. Neither damage nor residual deformation was observed in the SMAUD-based isolators at the end of the shake table tests, making them reusable throughout the entire tests without the need for repairs. By contrast, the SUD-based isolators exhibited apparent residual deformation under strong earthquakes.
(2) With the protection of the SMAUD-based isolators, the tested MRF model withstood nine consecutive ground motions and returned to its initial position with negligible residual drift ratios in each test. The entire steel MRF with SMAUD-based isolators demonstrated excellent seismic resilient performance during multiple strong earthquakes without evident damage, performance deterioration, or residual deformation.
(3) The numerical simulations could effectively capture the dynamic responses of the tested MRF and SMAUD-based isolators. The simulated time histories of roof displacement, inter-story drift ratios, and relative horizontal displacement of the isolators agreed well with the experimental results, indicating the accuracy and reliability of the proposed numerical model.
(4) Compared with the MRF with SUD-based isolators, the MRF with SMAUD-based isolators exhibited comparable peak dynamic response when subjected to the DBE level. More importantly, the SMAUD-based isolators achieved superior control over the SUD-based isolators on the residual deformation of the isolators owing to the flag-shaped hysteretic behavior of SMAUDs.
(5) The effect of the upper plate rotation of the isolator should also be considered, which contributed to a certain proportion of the overall frame responses. The effective inter-story drift ratios could be considerably smaller than the total inter-story drift ratio, which explains why the frame damage was very limited even after experiencing peak inter-story drift ratios exceeding 3.0%.

Meanwhile, some limitations of this study also need to be noted. This paper only discussed the seismic performance of the SMAUD-based isolators in an environment with stable room temperature when subjected to uni-directional ground motions. The effects of variable ambient temperatures in outdoor environments and multi-directional ground motions on the seismic performance of the proposed base isolators, together with those design improvements recommended in Section 5.5, warrant systematic future studies.

ACKNOWLEDGMENTS

The authors are grateful for the financial support from the Research Grants Council of Hong Kong through a GRF Project (Grant No. 15231723), the Hong Kong Branch of National Rail Transit Electrification and Automation Engineering Technology Research Center (Grant No. K-BBY1), and the Joint Research Centre for Marine Infrastructure (Grant No. 1-CEB0). The first author acknowledges the financial support from the Hong Kong PhD Fellowship Scheme. The findings and opinions expressed in this work are solely those of the authors and do not represent the views of the sponsors.

DATA AVAILABILITY STATEMENT

The data that support the findings of this study are available from the corresponding author upon reasonable request.

ORCID

Songye Zhu https://orcid.org/0000-0002-2617-3378
Bin Wang https://orcid.org/0000-0003-3595-5512
Zhi-peng Chen https://orcid.org/0009-0004-6030-6180

REFERENCES

1. Alavi B, Krawinkler H. Behavior of moment-resisting frame structures subjected to near-fault ground motions. *Earthq Eng Struct Dyn*. 2004;3(6):687-706.
2. Youssef NF, Bonowitz D, Gross JL. *A Survey of Steel Moment-Resisting Frame Buildings Affected by the 1994 Northridge Earthquake*. US National Institute of Standards and Technology; 1995.
3. Kelly JM. Base isolation: linear theory and design. *Earthq Spectra*. 1990;6(2):223-244.
4. Pan P, Zamfirescu D, Nakashima M, Nakayasu N, Kashiwa H. Base-isolation design practice in Japan: introduction to the post-Kobe approach. *J Earthq Eng*. 2005;9(01):147-171.
5. Buckle IG, Mayes RL. Seismic isolation: history, application, and performance—a world view. *Earthq Spectra*. 1990;6(2):161-201.
6. Suzuki K, Watanabe A, Saeki E. Development of U-shaped steel damper for seismic isolation system. *Nippon Steel Tech Rep*. 2005;92:56-61.
7. Ene D, Kishiki S, Yamada S, et al. Experimental study on the bidirectional inelastic deformation capacity of U-shaped steel dampers for seismic isolated buildings. *Earthq Eng Struct Dyn*. 2016;45(2):173-192.
8. Marquez J, Mosqueda G, Kim M. Modeling of lead rubber bearings under large cyclic material strains. *J Struct Eng*. 2021;147(11):04021170.
9. Providakis C. Effect of LRB isolators and supplemental viscous dampers on seismic isolated buildings under near-fault excitations. *Eng Struct*. 2008;30(5):1187-1198.
10. McCormick J, Aburano H, Ikenaga M, Nakashima M, Permissible residual deformation levels for building structures considering both safety and human elements. In: Proceedings of the 14th World Conference on Earthquake Engineering. Seismological Press Beijing; 2008.
11. Kalpakidis IV, Constantinou MC, Whittaker AS. Modeling strength degradation in lead–rubber bearings under earthquake shaking. *Earthq Eng Struct Dyn*. 2010;39(13):1533-1549.
12. Mokha A, Constantinou M, Reinhorn A, Zayas VA. Experimental study of friction-pendulum isolation system. *J Struct Eng*. 1991;117(4):1201-1217.
13. Jangid R, Kelly J. Base isolation for near-fault motions. *Earthq Eng Struct Dyn*. 2001;30(5):691-707.
14. Dicleli M. Performance of seismic-isolated bridges in relation to near-fault ground-motion and isolator characteristics. *Earthq Spectra*. 2006;22(4):887-907.
15. Constantinou MC, Tsopelas P, Kim Y, Okamoto S. NCEER-Taisei Corporation research program on sliding seismic isolation systems for bridges: experimental and analytical study of a friction pendulum system (FPS), 1993.
16. Lee GC, Ou Y-C, Niu T, Song J, Liang Z. Characterization of a roller seismic isolation bearing with supplemental energy dissipation for highway bridges. *J Struct Eng*. 2010;136(5):502-510.
17. Wang B, Zhu S, Chen K, Huang J. Development of superelastic SMA angles as seismic-resistant self-centering devices. *Eng Struct*. 2020;218:110836.
18. Fang C, Yam MC, Lam AC, Zhang Y. Feasibility study of shape memory alloy ring spring systems for self-centring seismic resisting devices. *Smart Mater Struct*. 2015;24(7):075024.
19. Dolce M, Cardone D. Mechanical behaviour of shape memory alloys for seismic applications 2. Austenite NiTi wires subjected to tension. *Int J Mech Sci*. 2001;43(11):2657-2677.
20. Miller DJ, Fahnestock LA, Eatherton MR. Development and experimental validation of a nickel–titanium shape memory alloy self-centering buckling-restrained brace. *Eng Struct*. 2012;40:288-298.
21. Qiu C, Zhu S. Shake table test and numerical study of self-centering steel frame with SMA braces. *Earthq Eng Struct Dyn*. 2017;46(1):117-137.
22. Zhu S, Zhang Y. Seismic analysis of concentrically braced frame systems with self-centering friction damping braces. *J Struct Eng*. 2008;134(1):121-131.
23. Speicher MS, DesRoches R, Leon RT. Experimental results of a NiTi shape memory alloy (SMA)-based recentering beam-column connection. *Eng Struct*. 2011;33(9):2448-2457.
24. Wang W, Fang C, Liu J. Self-centering beam-to-column connections with combined superelastic SMA bolts and steel angles. *J Struct Eng*. 2017;143(2):04016175.
25. DesRoches R, Taftali B, Ellingwood BR. Seismic performance assessment of steel frames with shape memory alloy connections. Part I—analysis and seismic demands. *J Earthq Eng*. 2010;14(4):471-486.
26. Li HN, Huang Z, Fu X, Li G. A re-centering deformation-amplified shape memory alloy damper for mitigating seismic response of building structures. *Struct Control Health Monit*. 2018;25(9):e2233.
27. Qiu C, Wang H, Liu J, Qi J, Wang Y. Experimental tests and finite element simulations of a new SMA-steel damper. *Smart Mater Struct*. 2020;29(3):035016.

28. DesRoches R, McCormick J, Delemont M. Cyclic properties of superelastic shape memory alloy wires and bars. *J Struct Eng*. 2004;130(1):38-46.
29. Dolce M, Cardone D, Marnetto R. Implementation and testing of passive control devices based on shape memory alloys. *Earthq Eng Struct Dyn*. 2000;29(7):945-968.
30. Choi E, Nam T, Oh J, Cho B. An isolation bearing for highway bridges using shape memory alloys. *Mater Sci Eng A Struct Mater*. 2006;438-440:1081-1084.
31. Casciati F, Faravelli L, Hamdaoui K. Performance of a base isolator with shape memory alloy bars. *Earthq Eng Eng Vib*. 2007;6(4):401-408.
32. Attanasi G, Auricchio F. Innovative superelastic isolation device. *J Earthquake Eng*. 2011;15(S1):72-89.
33. Fang C, Cao C, Zheng Y, Wu H, Wang W, Liang D. Self-centering energy-dissipative restrainers incorporating SMA ring springs. *J Struct Eng*. 2023;149(5):04023040.
34. Tamai H, Kitagawa Y. Pseudoelastic behavior of shape memory alloy wire and its application to seismic resistance member for building. *Comput Mater Sci*. 2002;25(1-2):218-227.
35. Sherif MM, Ozbulut OE. Tensile and superelastic fatigue characterization of NiTi shape memory cables. *Smart Mater Struct*. 2017;27(1):015007.
36. Wang B, Zhu S. Cyclic tension–compression behavior of superelastic shape memory alloy bars with buckling-restrained devices. *Constr Build Mater*. 2017;186:103-113.
37. Wang B, Zhu S, Casciati F. Experimental study of novel self-centering seismic base isolators incorporating superelastic shape memory alloys. *J Struct Eng*. 2020;146(7):04020129.
38. AISC. *Seismic Provisions for Structural Steel Buildings*. AISC Chicago; 2010.
39. ASCE. *Minimum Design Loads and Associated Criteria for Buildings and Other Structures. ASCE/SEI 7–16*. American Society of Civil Engineers; 2017.
40. Somerville PG. *Development of Ground Motion Time Histories for Phase 2 of the FEMA/SAC Steel Project*. SAC Joint Venture; 1997.
41. Lignos DG, Krawinkler H. Deterioration modeling of steel components in support of collapse prediction of steel moment frames under earthquake loading. *J Struct Eng*. 2011;137(11):1291-1302.
42. Gupta A, Krawinkler H. Estimation of seismic drift demands for frame structures. *Earthq Eng Struct Dyn*. 2000;29(9):1287-1305.
43. Moghadam SR, Konstantinidis D. Simple mechanical models for the horizontal behavior of elastomeric bearings including the effect of support rotation. *Eng Struct*. 2017;150:996-1012.
44. Ishii K, Kikuchi M, Nishimura T, Black CJ. Coupling behavior of shear deformation and end rotation of elastomeric seismic isolation bearings. *Earthq Eng Struct Dyn*. 2017;46(4):677-694.

How to cite this article: Huang J, Zhu S, Wang B, Chen Z. Shake table tests of steel moment resisting frame with self-centering SMA-based isolators. *Earthquake Engng Struct Dyn*. 2024;53:3489–3513.
https://doi.org/10.1002/eqe.4183